# Efficient determination of critical water activity and classification of hydrate-anhydrate stability relationship

Xin Yao[1]*, Tianyi Xiang[2], Shuang Chen[1], Busayo D. Alagbe[1], Richard S. Hong[1], Geoff G.Z. Zhang[1], Changquan Calvin Sun[2], Lian Yu[3], Ahmad Y. Sheikh[1]

1. Research & Development, AbbVie Inc., North Chicago, IL 60064, United States
2. Pharmaceutical Materials Science and Engineering Laboratory, Department of Pharmaceutics, College of Pharmacy, University of Minnesota, Minneapolis, Minnesota, MN 55455, United States
3. School of Pharmacy, University of Wisconsin-Madison, Madison, Wisconsin 53705, United States

# Abstract

For a pair of hydrated and anhydrous crystals, the hydrate is more stable than the anhydrate when the water activity is above the critical water activity ($a_{wc}$). Conventional methods to determine $a_{wc}$ are based on either hydrate-anhydrate competitive slurries at different $a_w$ or solubilities measured at different temperatures. However, these methods are typically resource-intensive and time-consuming. Here, we present simple and complementary solution- and solid-based methods for rapid determination of $a_{wc}$, using carbamazepine and theophylline as examples. In the solution-based method, $a_{wc}$ can be predicted using intrinsic dissolution rate (IDR) ratio or solubility ratio of the hydrate-anhydrate pair measured at a known water activity. In the solid-based method, $a_{wc}$ is predicted as a function of temperature from the dehydration temperature and enthalpy obtained by differential scanning calorimetry (DSC) near a water activity of unity. For carbamazepine and theophylline, the methods yielded $a_{wc}$ values in good agreement with those from the conventional methods. By incorporating $a_{wc}$ as an additional variable, the hydrate-anhydrate relationship is categorized into four classes based on their dehydration temperature ($T_d$) and enthalpy ($\Delta H_d$) in analogy with the monotropy/enantiotropy classification for crystal polymorphs. In Class 1 ($\Delta H_d < 0$ and $T_d \geq 373$ K), no $a_{wc}$ exists. In Class 2 ($\Delta H_d > 0$ and $T_d \geq 373$ K), $a_{wc}$ always exists under conventional crystallization conditions. In Class 3 ($\Delta H_d < 0$ and $T_d < 373$ K), $a_{wc}$ exists when $T > T_d$. In Class 4 ($\Delta H_d > 0$ and $T_d < 373$ K), $a_{wc}$ exists only when $T < T_d$. The hydrate-anhydrate pairs of carbamazepine and theophylline belong to Class 4.

# Introduction

Hydrates of active pharmaceutical ingredients (APIs) are prevalent in drug development, accounting for 20% of the top 100 best-selling drugs from 2005-2015.[1] In a survey by a contract research organization (CRO), 38% of solid-form screens (180 in total) observed hydrates.[2] The general existence of hydrates is attributed to the small size of water molecule and its ability to stabilize crystal lattice by efficiently forming H-bonds.[2,3] Given the different physical properties of hydrates relative to anhydrates,[3,4,5,6] e.g., generally lower water solubility in the pharmaceutically relevant temperature range, understanding their stability and transformation is important in drug development.

Critical to the characterization of a hydrate-anhydrate pair is their critical water activity ($a_{wc}$). This is akin to establishing the thermodynamic stability relationship of crystal polymorphs as a function of temperature,[7,8,9,10,11,12] but for a hydrate-anhydrate system, the water activity ($a_w$) is an additional variable.[7,13,14] By incorporating $a_{wc}$, it is interesting to discuss the hydrate-anhydrate stability relationship in analogy with the monotropy/enantiotropy classification for crystal polymorphs.[7,8] To measure $a_{wc}$, the competitive slurry method is considered the gold standard.[13] However, it only brackets $a_{wc}$ without giving a numeric value[15] and form conversion can be extremely slow near the $a_{wc}$.[16] To reach the precision of the second decimal place, typically 15-20 slurries are required at a single temperature.[16,17,18,19,20] Extrapolating solubility of a hydrate and an anhydrate at multiple temperatures based on the Van't Hoff equation, the transition temperature can be determined.[21] Both methods described above require intensive work and grams of materials, making them impractical in the early stage of drug development.

More recently, $a_{wc}$ determinations based on the intersection of IDR against $T$ or $a_w$ data [15] and an equation of solubility ratio derived from equilibrium constant have been reported[17] to reduce materials and experimental time. In-silico capabilities are also emerging as powerful tools to understand the complex dehydration behavior of hydrates,[22] and predict hydrate structures[23,24] with predicted $a_{wc}$ within one standard deviation (σ) of error.[24]

This work demonstrates a material-sparing and expedited experimental methodology to determine the $a_{wc}$ of a hydrate-anhydrate pair. The methods utilize the IDR (or solubility) ratio of a hydrate-anhydrate pair measured at a known water activity or the dehydration temperature and enthalpy measured by DSC near a water activity ($a_w$) of unity. For carbamazepine (CBZ) and theophylline (TPL), the results of these methods agree with those of the conventional methods. By incorporating $a_{wc}$ as an additional variable, the hydrate-anhydrate relationship is categorized into four classes based on their dehydration temperature and enthalpy in analogy with the monotropy/enantiotropy classification for polymorphs.

# Theoretical Section

For a pair of hydrate-anhydrate, $W_mB$(s) and $B$(s), equilibrated at a given critical water activity ($a_{wc}$) and temperature ($T$), $W_mB(s) \leftrightarrows B(s) + mW_c$, where $W_c$ is water molecules at $a_{wc}$, $B$ is the compound of interest, $m$ is the stoichiometry, and $s$ denotes solid, Eq. 1 stands:

$$\Delta G_d = \mu_{B(s)} + m\mu_{wc} - \mu_{W_mB(s)} = 0 \qquad \text{Eq. 1}$$

where $\mu_{W_mB(s)}$, $\mu_{B(s)}$, and $\mu_{wc}$ are the chemical potentials of $W_mB$(s), $B$(s), and water molecules at $a_{wc}$, respectively.

By expanding $\mu_{wc} = RT \ln a_{wc} + \mu_{w0}$, we get:

$$mRT \ln a_{wc} = \mu_{W_mB(s)} - \mu_{B(s)} - m\mu_{w0} = -\Delta G_{d0} \qquad \text{Eq. 2}$$

where $\mu_{w0}$ is the chemical potential of pure water.

Thus, finding the $a_{wc}$ is equivalent to determining the standard free energy change, $\Delta G_{d0}$, for the reaction, $W_mB(s) \rightarrow B(s) + mW_0$, where $W_0$ denotes pure water.

The derivation can be unfolded for a pair of two anhydrates if needed.

**Solution-based method**

If the solubilities of $W_mB$(s) and $B$(s) have been measured at the same $a_w$ and $T$, it can be shown:[17]

$$\ln a_{wc} = \frac{1}{m} \times \ln \frac{x_{B(mW)}}{x_B} + \ln a_w \qquad \text{Eq. 3}$$

where $x_{B(mW)}$ and $x_B$ are the solubilities of $W_mB$(s) and $B$(s). In deriving Eq. 3, it is assumed that the activity coefficients for $B$ are identical in the saturated solutions of the $W_mB$(s) and $B$(s).

If the solubilities or IDRs are measured in (nearly) pure water, i.e., $a_w \sim 1$, Eq. 3 is simplified to:

$$\ln a_{wc} \approx \frac{1}{m} \times \ln \frac{x_{B(mW)}^{a_w=1}}{x_B^{a_w=1}} \qquad \text{Eq. 4}$$

The assumption of $a_w \sim 1$ is generally valid except for highly water-soluble drugs (e.g., small sugar molecules). A high drug solubility in water can only cause overestimated $a_{wc}$ because $\ln a_w \leq 0$.

We can also replace the solubility ratio in Eqs. 3, 4 by the ratio of intrinsic dissolution rates (IDRs),[15] $\frac{x_{B(mW)}}{x_B} \approx \frac{IDR_{B(mW)}}{IDR_B}$.

**Solid-based method**

We now consider an alternative approach to determine $a_{wc}$, where the $\Delta G_{d0}$ is calculated as a function of temperature. Assuming that we can measure the dehydration process of $W_mB$(s) *in pure water under an equilibrium condition*, we have $\Delta G_{d0} = 0$ at the equilibrium dehydration temperature, $T_d$. We can obtain $\Delta G_{d0}$ at a lower temperature $T$ by integration:

$$\Delta G_{d0} = \Delta H_d \left(\frac{T_d - T}{T_d}\right) + \int_{T_d}^{T} \Delta C_p \cdot dT - T \times \int_{T_d}^{T} \Delta C_p \cdot dlnT \qquad \text{Eq. 5}$$

where $\Delta H_d$ is the enthalpy of dehydration and $\Delta C_p$ is the specific heat capacity change of dehydration, $\Delta C_p = C_{p,B(s)} + mC_{p,W_0} - C_{p,w_mB(s)}$. Thus, one can get:

$$\ln a_{wc} = \frac{-\left[\Delta H_d\left(\frac{T_d - T}{T_d}\right) + \int_{T_d}^{T} \Delta C_p \cdot dT - T \times \int_{T_d}^{T} \Delta C_p \cdot dlnT\right]}{mRT} \qquad \text{Eq. 6}$$

Assuming $\Delta C_p$ is a constant, we obtain:

$$\ln a_{wc} \approx \frac{-\Delta H_d}{mR}\left(\frac{1}{T} - \frac{1}{T_d}\right) + \frac{\Delta C_p}{mR} \times \left(\frac{T_d}{T} + ln\frac{T}{T_d} - 1\right) \qquad \text{Eq. 7}$$

Assuming $\Delta C_p = 0$, the equation can be simplified to:

$$\ln a_{wc} \approx \frac{-\Delta H_d}{mR}\left(\frac{1}{T} - \frac{1}{T_d}\right) \qquad \text{Eq. 8}$$

In practice, this method entails measuring $T_d$ and $\Delta H_d$ by DSC using water-saturated $W_mB$(s) in a hermetically sealed pan. Furthermore, $W_mB$(s) and $B$(s) should be sparingly water soluble at

$T_d$ so that the surrounding water activity is maintained near unity. Deviation from this condition (e.g., leakage of water vapor during measurement) would lead to erroneous results.

## Classification of hydrate-anhydrate stability relationship

Based on Eq. 8, there are four different situations according to $T_d \geq T_b$ (boiling point of water ≈ 373 K at 1 atm pressure) or not, and $\Delta H_d > 0$ or $\Delta H_d < 0$, as depicted in Figure 1. Under atmospheric pressure, the physical meaning exists only when $a_{wc} \leq 1$ and $T \leq 373$ K (the experimental quadrant is marked in red).

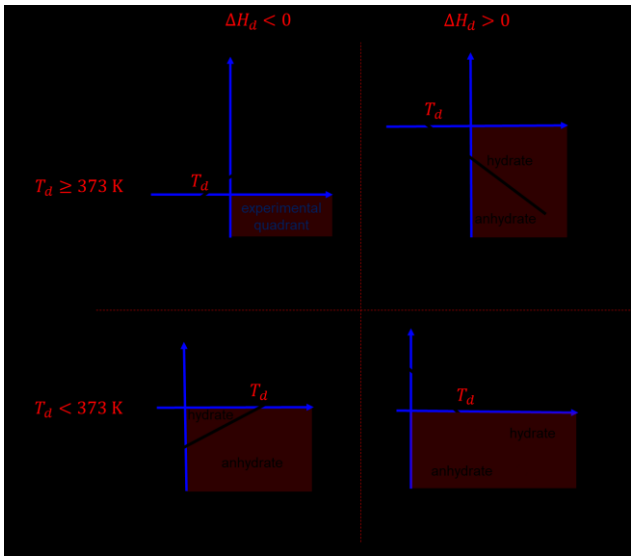


**Figure 1**. Four theoretical classes of ln $a_{wc}$ vs. $1/T$ based on $T_d \geq T_b$ (boiling point of water ≈ 373 K at 1 atm pressure) or not, and $\Delta H_d \geq 0$ or not. Under 1 atm pressure, the physical meaning exists only when $a_{wc} \leq 1$ and T ≤ 373 K (the quadrant is marked in red). Thus, in Class 1, no $a_{wc}$ exists. In Class 2, $a_{wc}$ always exists. In Class 3, $a_{wc}$ exists when $T > T_d$. In Class 4, $a_{wc}$ exists when $T < T_d$.

In Class 1 ($\Delta H_d < 0$ and $T_d \geq 373$ K), no $a_{wc}$ exists. The hydrate $W_mB$(s) is always less stable than the anhydrate $B$(s).

In Class 2 ($\Delta H_d > 0$ and $T_d \geq 373$ K), $a_{wc}$ always exists below 373 K.

In Class 3 ($\Delta H_d < 0$ and $T_d < 373$ K), $a_{wc}$ exists when $T > T_d$. It is counterintuitive that a hydrate can be more stable than its anhydrate at higher temperatures and less stable at lower temperatures. However, there is no theoretical reason to rule it out.

In Class 4 ($\Delta H_d > 0$ and $T_d < 373$ K), $a_{wc}$ exists only when $T < T_d$.

The classification can be determined if $a_{wc}$ is measured at multiple temperatures, as demonstrated using CBZ and TPL in this work.

# Materials and Methods

## Materials

CBZ anhydrate Form III and TPL anhydrate Form II were purchased from Sigma-Aldrich. CBZ dihydrate and TPL monohydrate were prepared by slurring the purchased solids in pure water at room temperature for one week. The hydrates were recovered by filtration and air-dried at 21 °C and ~40% RH for two days.

## Intrinsic Dissolution Rate

The intrinsic dissolution rate (IDR) was measured using the rotating disc method.[25] Each powder was compressed at a force of 1000 lb, using a custom-made stainless-steel die, against a flat stainless steel disc for 2 min to prepare a pellet (6.39 mm in diameter). The obtained pellet had a visually smooth surface that was coplanar with the surface of the die. While rotating at 300 rpm, the die was immersed in 300 mL of the dissolution medium at different temperatures in a water-jacketed beaker. A UV-vis fiber optic probe (Ocean Optics, Dunedin, FL) was used to continuously monitor the UV absorbance of the solution at $\lambda = 287$ nm, which was converted to a concentration-time profile based on a previously constructed concentration-absorbance standard curve. The initial linear part of the dissolution curve was used for calculating IDR.

## Powder X-ray Diffractometry

PXRD data were collected using an ARL EQUINOX 3500 (Thermo Fisher Scientific Inc., Waltham, MA) equipped with a CPS 590 detector and a Cu microfocus source. The

diffractometer was operated with a copper anode tube at 40 kV and 30 mA. XRD data were collected from 0–90° 2θ with an integration time of 600 s.

Differential Scanning Calorimetry (DSC)

DSC experiments were performed with a TA DSC2500 under 50 mL/min $N_2$ purge. For measuring the enthalpy of dehydration ($\Delta H_d$), CBZ dihydrate or TPL monohydrate crystals (3-7 mg) were placed in a T-zero pan. After the mass of each sample was measured, 0.5 µL water was added into the pan, and the pan was hermetically sealed. The samples were heated to 90 °C at 1 K/min. $T_d$ and $\Delta H_d$ are measured as the very onset and the integration of the dehydration peak. We tested the amounts of 2, 1, 0.5 and 0 µL water and the difference in measured $\Delta H_d$ and $T_d$ is negligible.

The change in specific heat capacity ($\Delta C_p$) of dehydration was measured using the modulated mode. The sample preparation is similar to the normal DSC samples except that after the dry powders of CBZ dihydrate and TPL monohydrate were loaded in T-zero pans, the powder was pressed with a stainless-steel punch to ensure good contact with the pan and flat surface of the powder bed. After that, 0.5 µL water was added into each sample and the pan was hermetically sealed. The $\Delta C_p$ before and after dehydration were measured using the modulated DSC (sinusoidal temperature modulation with an amplitude of 0.25 K and a period of 60 s) with a heating or cooling rate of 1 K/min. The samples were cooled and heated by multiple cycles before dehydration temperature and after dehydration. After dehydration, rehydration has not

been observed during the heat-cool cycles. The reversing heat capacities are repeatable at different cycles, indicating the reliability of measured $\Delta C_p$ data.

## Solubility determination

The solubility of CBZ Form III and TPL Form II was measured by plotting the concentration vs. dissolution time and averaging the plateau region before solids fully converted to hydrates. Since the two anhydrates convert to hydrates quickly at low temperatures relative to the transit temperature, the water or water solutions need to be preequilibrated at the targeted temperature. The solutions were drawn out every ~60 s and passed through a 0.45 μm syringe filter, which is pre-equilibrated at the targeted temperature as well. The filtrate was collected in a heated vial at 60 °C to avoid recrystallization due to temperature drop. The filtrates then were diluted 10 times in acetonitrile (ACN) for CBZ and in water/ACN (1 : 1, v/v) for TPL. The samples were analyzed using HPLC. The solubility of hydrates is measured conventionally. The slurries of hydrates were kept at the targeted temperature while being stirred. Samples were collected after 1 day equilibrium. The filtrates were treated and analyzed in the same way as described above.

## Single-point DFT calculation of relevant energies of dehydration

The interaction energies of both the host molecules and water were evaluated using single-point dispersion-corrected density functional theory (DFT-D) calculations on the optimized experimental structures of CBZ Form III (CBMZPN01),[26] CBZ dihydrate (FEFNOT02),[27] TPL Form II (BAPLOT06),[28] and TPL monohydrate (THEOPH05).[29] Single point energetics were evaluated on the optimized experimental structures, the optimized structures with water

molecules removed, as well as the conformers of host molecules and water molecules from the crystal structure. The optimizations and energy calculations were performed using the PBE functional[30] with the Neumann-Perrin (NP) dispersion correction,[31] a plane wave basis set (520 eV, $2\pi \times 0.07$ Å-1 k-point grid) and default PAW pseudopotentials, as implemented in VASP 6.2.1.[32,33,34] The single point calculation of the individual water and host molecules was performed using a 30 Å x 30 Å x 30 Å cell such that only the atomic and intramolecular energies of the individual molecules are captured. The methodology utilized to determine the data reported in Table 3. is as follows:

$$Host\ only\ energy\ = \frac{E_{crys\_no\_water}}{N_{host}}$$

$$Water\_involved\ energy\ = \frac{E_{opt\_cryst}\ -\ E_{crys\_no\_water}}{N_{water}}$$

$$Single\ host\ molecule\ =\ E_{host\_molecule}$$

$$Host\_host\ Interactions\ = \frac{E_{crys\_no\_water}}{N_{host}}\ - E_{host\_molecule}$$

$$Water\_involved\ interactions = \frac{E_{opt\_cryst}\ -\ E_{crys\_no\_water}}{N_{water}}\ - E_{water}$$

Where,

$E_{crys\_no\_water}$ = energy of optimized experimental structure with no waters

$N_{host}$ = number of host molecules in unit cell

$E_{opt\_cryst}$ = energy of optimized experimental structure

$N_{water}$ = number of water molecules in unit cell

$E_{host\_molecule}$ = energy of single host molecule

$E_{water}$ = energy of single water molecule

# Results

*Solution-based method*

The solubility of CBZ Form III and monohydrate in pure water is plotted against $T$ in Figure 1(a). CBZ Form III exhibits higher solubility than CBZ dihydrate below 340 K in pure water, indicating dihydrate is more stable than Form III within this temperature range. The IDRs of TPL Form II and monohydrate were measured in water/methanol (8/2 molar ratio) against $T$. The $a_w$ of water/methanol solution at multiple temperatures is reported,[35,36,37] and summarized in Table S2. The IDR of TPL Form II is higher than that of TPL monohydrate at and below 313 K but lower at 333 K, indicating the transition temperature is within 313-333 K in the water/methanol solution.

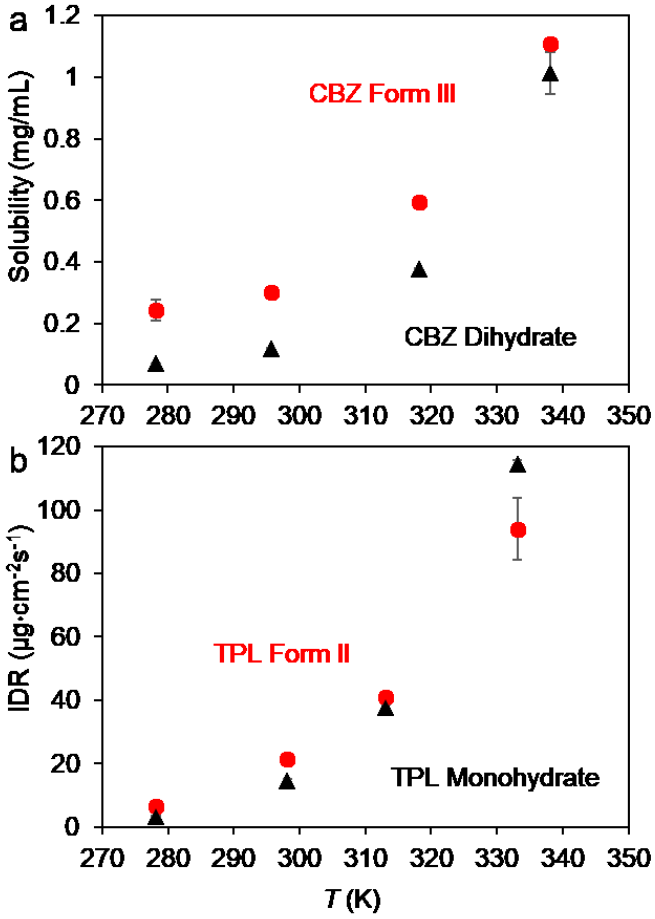


**Figure 1**. (a) Solubility of CBZ Form III and dihydrate in water vs. temperature and (b) IDR of TPL Form II and monohydrate in water/methanol at 8/2 molar ratio.

Using Eq. 3 or 4, the critical water activity ($a_{wc}$) is determined by inputting the solubility or IDR ratio measured in this work or from the literature for CBZ[15,17] and TPL,[17,38,39,40] which is summarized in Table S2. The $a_{wc}$ values are plotted as a function of temperature in Figure 2 with the values measured by conventional methods of competitive slurry [16,17,18,19,20,21] and extrapolating solubility (IDR) temperature profiles,[15,21] which are provided in Table S1. The $a_{wc}$ values measured by conventional methods from different labs are consistent. For CBZ, the $a_{wc}$ is between dihydrate and anhydrate Form III,[15,16,17] while it is between monohydrate and anhydrate Form II for TPL.[17,18]

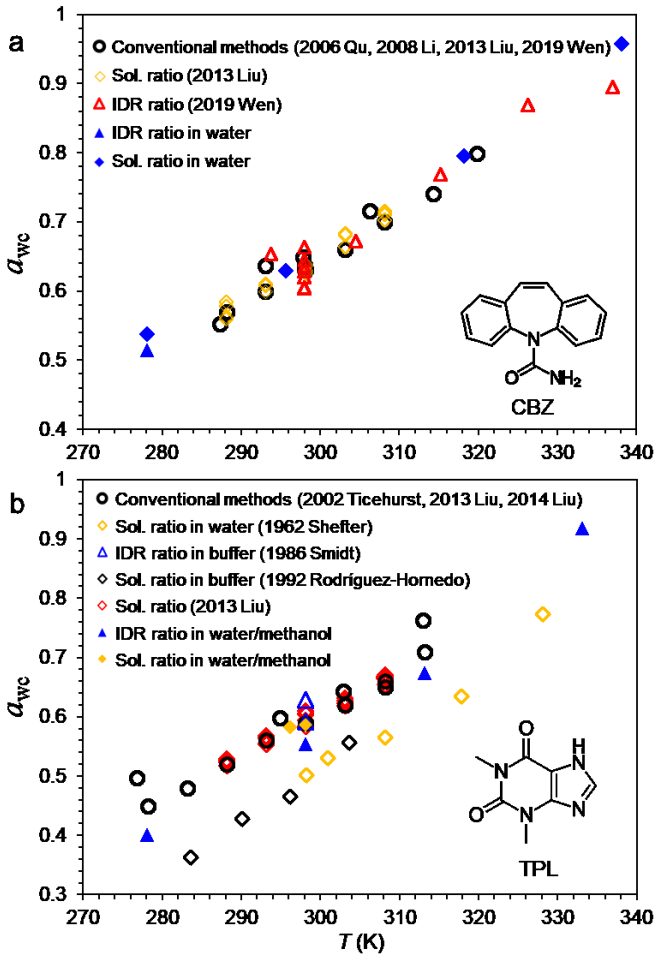


**Figure 2**. $a_{wc}$ calculated by the solution-state methods of CBZ (a) and TPL(b) vs. temperature, compared with that of conventional methods. $a_{wc}$ values (black open circles) determined by conventional methods (slurry, solubility and IDR extrapolation) in different labs are consistent within error. The calculated $a_{wc}$ based on IDR (triangles) or solubility (diamonds) ratio agrees with that of the conventional methods within an error of ±0.03 for CBZ. The bigger error on TPL is likely caused by significant change of activity coefficient and its low water stoichiometry (monohydrate).

The $a_{wc}$ values determined using IDR (solubility) ratios for CBZ agree with the values within an error of 0.03, which is comparable to the error of conventional methods. However, in the case of TPL, the error is relatively larger, where the prediction from the solubility data in water or buffer shows a systematically negative deviation (~ -0.1). This discrepancy is likely due to the significant difference in activity

coefficient of TPL in aqueous solutions saturated with monohydrate and Form II. Likely, the significant change of activity coefficient happens when solute molecules start to self-assemble into molecular complexes.

The decrease of water activity in pure water by dissolved CBZ or TPL can be ignored. The solubility of CBZ is lower than that of TPL. The molar concentration of TPL is ~0.3% (~30 mg/mL) at 323 K in water, falling within the water-soluble category. The decrease of $a_w$ caused by TPL should be within 0.01.

A significant factor contributing to the bigger error in TPL is its low water stoichiometry. Assuming the errors in solubility or IDR are similar for different drugs, the errors will directly transfer to the $a_{wc}$ in the monohydrate case, but will decrease significantly for higher hydrates, based on Eqs. 3 and 4. For example, if the error of the solubility and IDR ratio is 10%, the error of $a_{wc}$ is also 10% in the monohydrate case but will be only 5% in the dihydrate case.

Since CBZ and TPL are not strong acids or bases, the pH change caused by solubility difference is negligible. For ionizable drugs, their solubility depends on pH, but the solubility ratio is independent of pH because the ionic species have the same distribution at a given pH. The consistent solubility ratio in water and pH buffer of CBZ and TPL confirms this. However, using a buffer, instead of water, to maintain a constant pH of the solutions saturated by different solids would likely yield more accurate results for ionizable drugs.

*Solid-based method*

Here, we demonstrate that $a_{wc}$ can be determined by measuring the dehydration temperature ($T_d$) and enthalpy ($\Delta H_d$) in DSC, based on Eqs. 6-8. Recall that $T_d$ and $\Delta H_d$ are specified values in pure water ($a_w = 1$). Therefore, hydrates were hermetically sealed in DSC pans with a small amount of water. As shown in Figure 3, dehydration of CBZ and TPL happens with a sharp endothermic peak in a hermetically sealed pan but a very broad peak in a pierced pan. In a sealed pan, $T_d$ is the onset and $\Delta H_d$ is the integration of the endothermic peak, as shown in Figure 3. The values are summarized in Table 1. In a pierced pan, the physical meaning of the onset temperature is ambiguous because the surrounding RH is unknown due to $N_2$ flow and gas exchange. Dehydration may happen slowly at the beginning indicated by the slope of the baseline of the pierced samples. Additionally, the heat change in a pierced pan includes the enthalpy of water evaporation. Consequently, the heat change in a pierced pan is several times that of the sealed pan, as shown in Table 1.

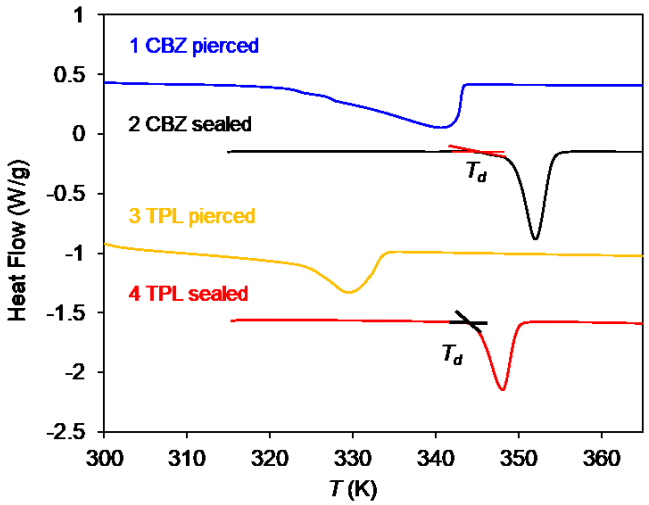


**Figure 3**. DSC heating traces of dihydrate CBZ and monohydrate TPL in pierced and hermetically sealed pans. Dehydration happens with an endothermic peak. $T_d$ can be measured as the very onset, and $\Delta H_d$ is the integration of endothermic peak using the traces in sealed pans. In pierced pans, the dehydration peaks are much broader and happens much earlier.

The phases of CBZ and TPL after dehydration are identified using PXRD, as shown in Figure 4. The dehydrated solid in DSC pans are Form III for CBZ and Form II for TPL. The measured hydrate-anhydrate pairs in DSC match the transition pairs in the solution-based method.

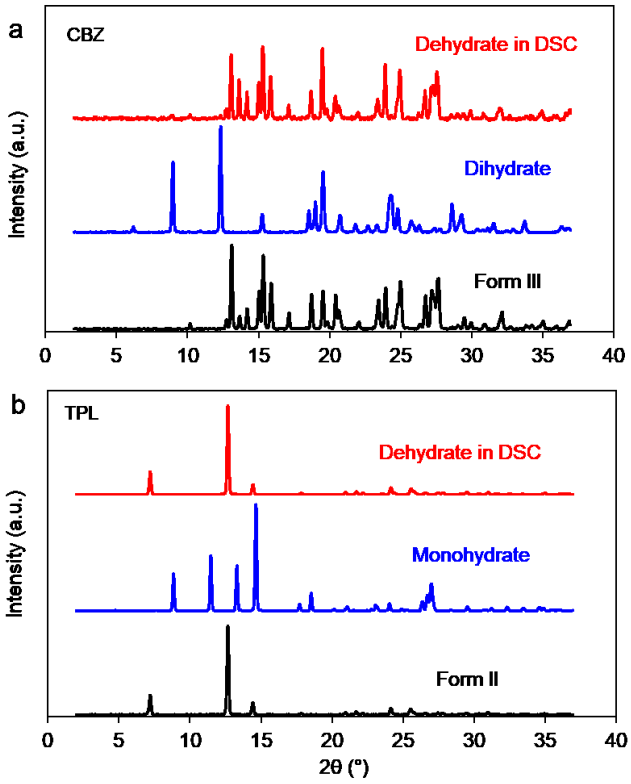


**Figure 4**. PXRD patterns of the CBZ (a) and TPL (b) anhydrates, hydrates, and their dehydrate forms in DSC, from bottom to top. PXRD results indicate that CBZ dihydrate converts to Form III, and TPL monohydrate converts to Form II after dehydration.

The measured $T_d$s of TPL and CBZ are lower than 373 K and their $\Delta H_d$s are positive (see Table 1), indicating the hydrate-anhydrate pairs of CBZ and TPL are Class 4, which is consistent with the $a_{wc} - T$ profiles measured by the solution-based method. The positive relationship between $a_{wc}$ and $T$ is equivalent to $\Delta H_d > 0$, and the extrapolation to $a_{wc} = 1$ indicates $T_d < 373$ K (Figure 2).

The heat capacity change of dehydration ($\Delta C_p$), measured by modulated DSC, is plotted as the $\Delta C_p$ per mole water ($\Delta C_p/m$) against temperature and compared with that of ice melting linearly extrapolated from subzero data (Figure 5). It is worth noting that the $\Delta C_p/m$ of dehydration is less than that of ice melting. The $\Delta C_p$ of dehydration can be taken as the sum of the heat capacity change of molecule (B) at different solid states and that of water liquefying from hydrates. Since

the heat capacity change of the organic molecule (B) at different solid states is usually small, the $\Delta C_p$ of dehydration mainly depends on the heat capacity change of water. It can be understood that the $\Delta C_p$ of dehydration is less than that of ice melting, considering water molecules in ice have the lowest freedom among all the solid states of water molecule by forming 4 ideal hydrogen bonds per molecule. In the crystal lattice of dihydrate CBZ and monohydrate TPL,[26,27,28,29] the H-bonds formed by $H_2O$ are summarized in Table 2. The H-bonds have unideal angles, and the average H-bonds per $H_2O$ is 3.5 in CBZ dihydrate and 3 in TPL monohydrate, indicating higher freedom and thus higher heat capacity than ice. The averaged $\Delta C_p/m$ was calculated as 20 J/mol/K for CBZ and 14 J/mol/K for TPL within the temperature range of 278-348 K.

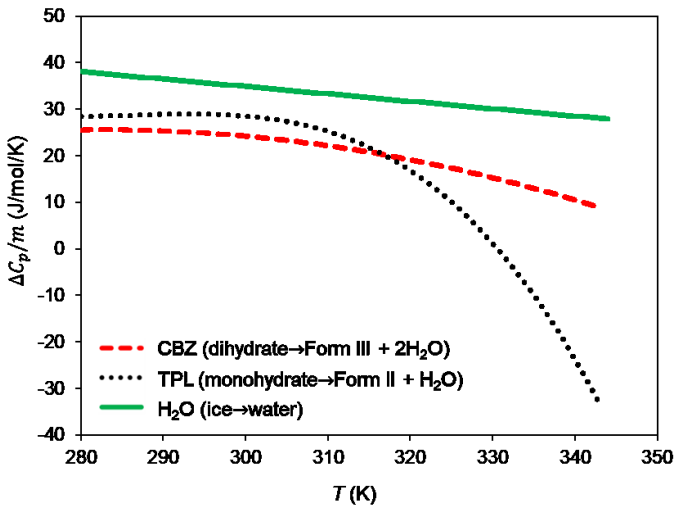


**Figure 5**. Heat capacity change per mole water ($\Delta C_p/m$) of the dehydration of CBZ and TPL in a common process temperature range, compared with that of ice melting extrapolated from subzero data. The $\Delta C_p/m$ of dehydration is less than that of ice melting.

**Table 1.** $T_d$ and $\Delta H_d$ of CBZ and TPL measured from DSC heating traces in hermetically sealed pans with the peak range ($T_{pierced}$) and enthalpy change $\Delta H_{pierced}$ of dehydration in pierced pans.

| | Transition | $T_d$ (K) | $\Delta H_d$ (J/mol) | $T_{pierced}$ (K) | $\Delta H_{pierced}$ (J/mol) |
|---|---|---|---|---|---|
| CBZ | Dihydrate to anhydrate Form III | 345 ± 3 | 17314 ± 1530 | 320-343 (broad peak) | ~74443 |
| TPL | Monohydrate to anhydrate Form II | 343 ± 1 | 9297 ± 351 | 310-333 (broad peak) | ~47642 |

**Table 2.** H-bonds of water molecules in CBZ dihydrate and TPL monohydrate.

| | H-bond with water involved | The donor and acceptor of H-bonds | Angle (°) | O-O distance (Å) |
|---|---|---|---|---|
| CBZ dihydrate (FEFNOT02) | H-bond1 | O1-H···O=C-R (CBZ) | 158.02 | 2.831 |
| | H-bond2 | O1-H···O2 | 176.97 | 2.886 |
| | H-bond3 | O2-H···O1 | 166.12 | 2.936 |
| | H-bond4 | O2-H···O1 | 172.09 | 2.815 |
| | | | | |
| TPL monohydrate (THEOPH05) | H-Bond1 | O-H···N (TPL) | 167.72 | 2.898 |
| | H-Bond2 | O-H···O | 168.36 | 2.724 |
| | H-Bond3 | O-H···O | 162.38 | 2.744 |

**Table 3.** Host-host interactions and water-involved interactions of CBZ and TPL crystals from Single-Point DFT-D Calculations.

| | Host only energy (kJ/mol) | Water-involved energy (kJ/mol water) | Single host molecule energy (kJ/mol) | Host-host Interactions (kJ/mol) | Water-involved interactions (kJ/mol water) |
|---|---|---|---|---|---|
| CBZ Form III | -19741.9 | N.A. | -19590.7 | -151.2 | N.A. |
| CBZ dihydrate | -19717.4 | -1456.0 | -19587.7 | -129.7 | -87.1 |
| TPL Form II | -13675.8 | N.A. | -13524.4 | -151.4 | N.A. |
| TPL monohydrate | -13660.7 | -1440.5 | -13526.9 | -133.8 | -71.6 |

The $a_{wc}$ was calculated by substituting the DSC data ($T_d$, $\Delta H_d$, and $\Delta C_p$) into Eqs. 6-8, and compared to the values from other methods by plotting ln($a_{wc}$) against inverse temperature, as shown in Figure 6. The black dots are $a_{wc}$ values determined from slurry, solubility, and IDR data. The open green circles are calculated using Eq. 6 with measured $\Delta C_p$. The blue lines with open triangles are plotted using Eq. 7 by considering $\Delta C_p$ as a constant, and the red lines with open diamonds are plotted using Eq. 8 by assuming $\Delta C_p$ as 0. The three equations coincide at temperatures close to the $T_d$ and diverge slightly with decreasing temperature, but the difference of $a_{wc}$ is still within 0.3 around 295 K. Thus, the assumption of ignoring the heat capacity change is reasonable for CBZ and TPL. The linear relationship has also been observed for gabapentin.[14] The assumption should be generally valid because the heat capacity change is capped by that of ice melting (<35 J/mol/K). The $a_{wc}$ values determined by Eq. 6-8 using DSC data agree well with that from the slurry, solubility, and IDR data within experimental error along the whole temperature range as shown in Figure 6.

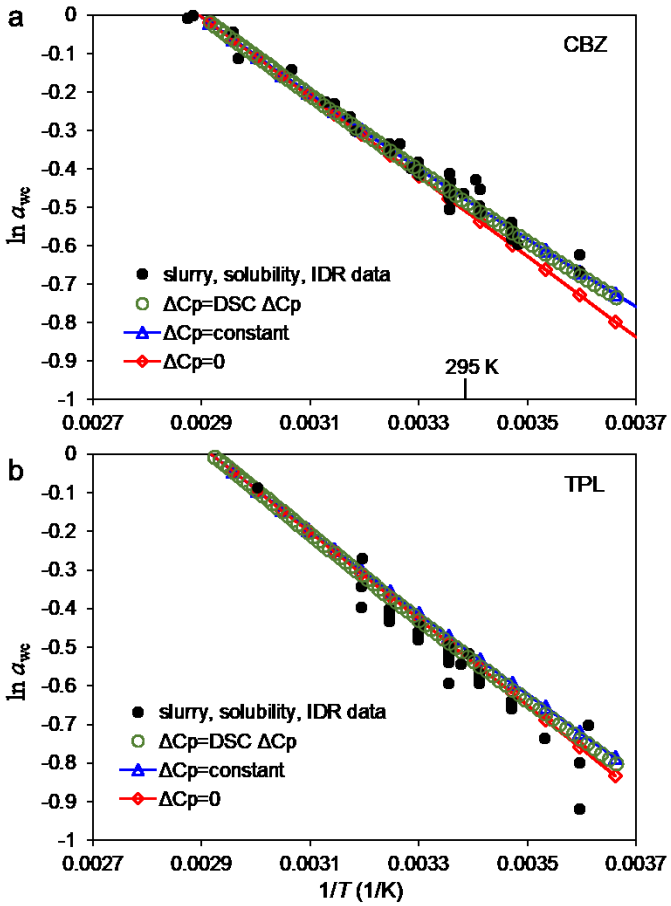


**Figure 6**. Predicted $a_{wc}$ using DSC data ($T_d$, $\Delta H_d$, and $\Delta C_p$) of CBZ (a) and TPL (b), plotted with $a_{wc}$ from slurry, solubility, and IDR data. The TPL solubility data in water is excluded for its systematic deviation. The green open circles are the predicted $a_{wc}$ using Eq. 6 and the measured $\Delta C_p$ by modulated DSC, the blue curves with open triangles are plotted using Eq. 7 by considering $\Delta C_p$ as a constant, and the red curves with open diamonds are plotted using Eq. 8 by assuming $\Delta C_p$= 0.

To understand the enthalpy change during dehydration, single-point DFT-D calculation[22] was conducted. The host-host interactions and water-involved interactions (the sum of host-water and water-water interactions) were calculated (See Table 3). The ratio of water-involved interactions between the CBZ dihydrate and TPL monohydrate (-87.1 (kJ/mol) /-71.6 (kJ/mol)) is very close to the ratio of their average H-bonds number per water molecule (3.5/3). The host-host interactions of the hydrates are lower than that of the anhydrates for both CBZ and TPL because the host molecules pack less densely in hydrates due to the voids occupied by water molecules. The single-molecular energy is similar between hydrates and anhydrates, consistent with their crystal structures.[26,27,28,29] Thus, during dehydration, the host molecules repack to lower their enthalpy without significant conformation change. However, the dehydration process is an endothermic process. Thus, the water-involved enthalpy increase must compensate for the enthalpy decrease of the host-only part during dehydration, indicating the importance of water molecules in stabilizing the hydrates.

# Discussion

We compare the methods for determining $a_{wc}$ in this work (Table 4). The competitive slurry method is considered the gold standard with the lowest limitation. However, it requires a few grams of material and intensive work to achieve reasonable precision. The DSC method is the most material sparing and fastest, but also requires dehydration to the interested anhydrous form. This limitation can be mitigated by incorporating the free energy difference of two anhydrates, which has been demonstrated previously.[7,8,13]

The solubility ratio and IDR ratio methods require a higher workload than the DSC method but still much lower than the competitive slurry method. They are particularly useful for studying the full thermodynamic landscape of multiple solid forms. The workload of these two methods increases proportionally with the number of solid forms ($N$). In comparison, the slurry method requires $C_N^2$ pairs of slurry series and the DSC method likely cannot work due to uncontrolled forms after dehydration.

For solids having fast conversion in solution, the solubility ratio method can only work near the transition point, while IDR ratio method has less limitation. Since the IDR can be measured from the beginning of dissolution, even the $a_{wc}$ of labile crystals in solution can be determined using this method. However, the accuracy of IDR is typically lower than that of solubility, and this method is only suitable for stable crystals upon compression. Overall, the complementary methods offer diverse strategies based on data quality requirements and project timelines in drug development.

The methods described in this work are for determining $a_{wc}$ between a hydrate and an anhydrate, not between mixed-solvate hydrate and anhydrate. Hence, it is important to note the criticality of

identifying whether a hydrate is formed by desolvating an intermediate unstable mixed-solvate hydrate when applying the methods for crystallization process development. However, if needed, it is possible to incorporate the chemical potential of a third component into Eq. 1 to study mixed-solvate hydrates.

**Table 4.** Comparison of the methods in this work with the competitive slurry method.

| Method | Solubility ratio | IDR ratio | DSC data of dehydration | Competitive slurry |
|---|---|---|---|---|
| Material required | ~200 mg | ~500 mg | ~10 mg | grams |
| Result type | Numerical | Numerical | Numerical | Bracket |
| Time | days | days | hours | weeks |
| Limitation level & Requirements | Level 2<br>Slow form conversion in solution | Level 1<br>Stable solids under compression | Level 3<br>Dehydration to the target anhydrous form | Level 0<br>Significant amount of material and workload |
| Workload for $N$ number of solid forms | $N$ solubility measurements | $N$ IDR measurements | Likely cannot work for any pair of two solids | $C_N^2$ pairs of slurry series |

The solubility (IDR) ratio of a hydrate-anhydrate pair in water can identify whether $a_{wc}$ exists. We plot $\ln\frac{x_{B(mW)}}{x_B} = \ln\frac{x_{B(mW)}^{a_W=1}}{x_B^{a_W=1}} - m\ln a_w$ derived from Eqs. 3 and 4, see Figure 7. According to the equation, a straight line with a slope of $m$ can be observed. $\ln a_{wc}$ is the intercept on $x$-axis, and $\ln\frac{x_{B(mW)}^{a_W=1}}{x_B^{a_W=1}}$ is the intercept on $y$-axis. At a given temperature, $\ln\frac{x_{B(mW)}^{a_W=1}}{x_B^{a_W=1}} \leq 0$ (Figure 8a) or $\ln\frac{x_{B(mW)}^{a_W=1}}{x_B^{a_W=1}} > 0$ (Figure 8b). Since only negative value of $\ln(a_w)$ is physically meaningful, $a_{wc}$ exists only if the anhydrate has higher solubility (IDR) than the hydrate in water, just like the cases of CBZ and TPL below $T_d$.

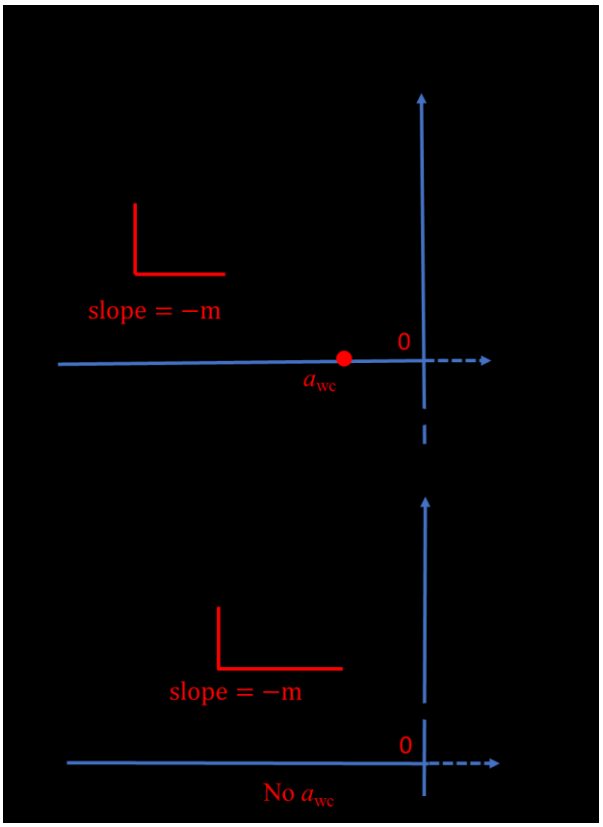


**Figure 7**. The diagram of the two cases of solubility (IDR) ratio in water at a given temperature. In Case 1 (a), $\ln\frac{x_{B(mW)}^{a_W=1}}{x_B^{a_W=1}} \leq 0$ and $a_{wc}$ exists. In Case 2 (b), $\ln\frac{x_{B(mW)}^{a_W=1}}{x_B^{a_W=1}} > 0$ and $a_{wc}$ does not exist.

As described in the theoretical section, the stability relationship of a hydrate-anhydrate pair can be categorized into 4 classes. The specific pairs of CBZ and TPL in this work fall into Class 4 ($\Delta H_d > 0$ and $T_d < 373$ K), where $a_{wc}$ exists when $T < T_d$. Likely, Class 4 is the most common situation for hydrate-anhydrate pairs where a relative stable hydrate exists. If the enthalpy contribution from host molecules is similar between the hydrate and anhydrate, their energy difference is relatively small compared with the water-involved enthalpy increase during

dehydration (see Table 3 for CBZ and TPL). Thus, the dehydration process is endothermic. The hydrates in Class 4 are more stable at lower temperatures and their drying at elevated temperature often requires humidification above their $a_{wc}$.

Dasabuvir[41] and morphine[42] are two examples of Class 2 hydrate-anhydrate pairs ($\Delta H_d > 0$ and $T_d \geq 373$ K), where $a_{wc}$ always exists under conventional crystallization conditions (< 373 K, 1 atm). Class 2 is relevant for highly stable hydrates with relatively low $a_{wc}$ at room temperature; e.g., monohydrate morphine ($\Delta H_d > 0$ and $T_d \geq 373$ K) barely dehydrates even at 0 RH and 298 K in dynamic vapor sorption (DVS),[42] indicating its relatively low $a_{wc}$ at 298 K. A Class 2 hydrate would be suitable for development from the solid form physical stability perspective. For example, a very stable monohydrate of Dasabuvir ($\Delta H_d > 0$ and $T_d > 383$ K)[41] was chosen as the commercial form, allowing simple drying without humidity control.

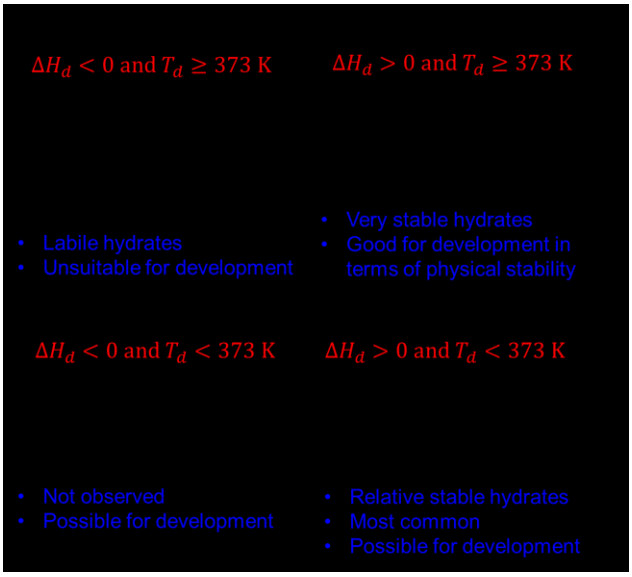

**Figure 9**. Four classes of hydrate-anhydrate pairs.

Classes 1 and 3 have exothermic dehydration reaction, which is not common. The negative $\Delta H_d$ can happen when the hydrate has very loose packing or high disorder relative to the anhydrate. The enthalpy released from host molecules during dehydration must compensate for the enthalpy absorbed for water liquefying. In Class 1 ($\Delta H_d < 0$ and $T_d \geq 373$ K), no $a_{wc}$ exists under conventional crystallization conditions (< 373 K, 1 atm). The Class 1 hydrate is always less stable than the anhydrate. Such labile hydrates may exist as kinetic forms or desolvated forms from mixed-solvate hydrates and would exhibit even higher solubility than the anhydrate in

444 water below 373 K, indicating they are less stable independent of $a_w$. A few Class 1 hydrates
445 have been observed in our internal form screening. Such labile hydrates are unsuitable for
446 development and have rarely been studied for a good reason.

447 In Class 3 ($\Delta H_d < 0$ and $T_d < 373$ K), $a_{wc}$ exists when $T > T_d$. Such hydrates are more stable at
448 higher temperatures. To the best of our knowledge, hydrate-anhydrate pairs in Class 3 have not
449 been previously reported. It will be very interesting to find a Class-3 example, as a Class 3
450 hydrate is suitable for solid-form development if its $T_d$ is low.

451

452 # Conclusions

453 Simple and complementary methods and a thermodynamic model for determining $a_{wc}$ are
454 illustrated using carbamazepine and theophylline. In the solution-based method, $a_{wc}$ can be
455 determined using intrinsic dissolution rate (IDR) ratio or solubility ratio of a hydrate-anhydrate
456 pair measured at a known $a_w$. In the solid-based method, $a_{wc}$ is predicted as a function of
457 temperature from the dehydration temperature and enthalpy obtained by DSC. These methods
458 yielded $a_{wc}$ values in good agreement with those from the conventional methods. Overall, the
459 complementary methods offer diverse strategies based on data quality requirements and project
460 timelines in drug development. Hydrate-anhydrate pairs are categorized into four classes with
461 examples based on whether $T_d \geq 373$ K and $\Delta H_d > 0$. It will be interesting to study whether the
462 thermodynamic model can be modified for non-stoichiometric hydrates or mixed-solvate
463 hydrates. It will also be enticing to unfold the solid-based method for a hydrate-anhydrate pair
464 whose $T_d$ and $\Delta H_d$ cannot be directly measured. More insights may be gained of an example of
465 Class 3 hydrate is discovered in drug development by applying the analysis in this .

## Supplementary Materials

The $a_{wc}$ values measured by conventional methods are summarized in Table S1 and the IDR and solubility data used for calculating $a_{wc}$ are summarized in Table S2.

## Acknowledgements

AbbVie funded the study and participated in study design, research, data collection, analysis and interpretation of data, writing, reviewing, and approving the publication. All authors have no additional conflicts of interest to report. X.Y., S.C., B.D.S., R.S.H., G.G.Z.Z. and A.Y.S. are employees of AbbVie and may own AbbVie stocks. CCS thanks the National Science Foundation for support through the Industry University Collaborative Research Center (IUCRC) grant IIP-2137264, Center for Integrated Materials Science and Engineering for Pharmaceutical Products (CIMSEPP).

## References:

[1] Damron, J.T., Kersten, K.M., Pandey, M.K., Nishiyama, Y., Matzger, A. and Ramamoorthy, A., 2017. Role of Anomalous Water Constraints in the Efficacy of Pharmaceuticals Probed by 1H Solid-State NMR. ChemistrySelect, 2(23), pp.6797-6800.
[2] Brini, E., Fennell, C.J., Fernandez-Serra, M., Hribar-Lee, B., Luksic, M. and Dill, K.A., 2017. How water's properties are encoded in its molecular structure and energies. Chemical reviews, 117(19), pp.12385-12414.
[3] Khankari, R.K. and Grant, D.J., 1995. Pharmaceutical hydrates. Thermochimica acta, 248, pp.61-79.

[4] Hong, R.S., Mattei, A., Sheikh, A.Y. and Tuckerman, M.E., 2022. A data-driven and topological mapping approach for the a priori prediction of stable molecular crystalline hydrates. Proceedings of the National Academy of Sciences, 119(43), p.e2204414119.
[5] Schneider-Rauber, G., Arhangelskis, M., Bond, A.D., Ho, R., Nere, N., Bordawekar, S., Sheikh, A.Y. and Jones, W., 2021. Polymorphism and surface diversity arising from stress-induced transformations–the case of multicomponent forms of carbamazepine. Acta Crystallographica Section B: Structural Science, Crystal Engineering and Materials, 77(1), pp.54-67.
[6] Schneider-Rauber, G., Arhangelskis, M., Goh, W.P., Cattle, J., Hondow, N., Drummond-Brydson, R., Ghadiri, M., Sinha, K., Ho, R., Nere, N.K. and Bordawekar, S., 2021. Understanding stress-induced disorder and breakage in organic crystals: beyond crystal structure anisotropy. Chemical Science, 12(42), pp.14270-14280.
[7] Gu, C.H. and Grant, D.J., 2001. Estimating the relative stability of polymorphs and hydrates from heats of solution and solubility data. Journal of pharmaceutical sciences, 90(9), pp.1277-1287.
[8] Yu, L., 1995. Inferring thermodynamic stability relationship of polymorphs from melting data. Journal of pharmaceutical sciences, 84(8), pp.966-974.
[9] Yao, C., Guzei, I.A., Jin, Y., Ruan, S., Sun, G., Gui, Y., Wang, L. and Yu, L., 2020. Polymorphism of piroxicam: new polymorphs by melt crystallization and crystal structure prediction. Crystal Growth & Design, 20(12), pp.7874-7881.
[10] Gui, Y., Yao, X., Guzei, I.A., Aristov, M.M., Yu, J. and Yu, L., 2020. A mechanism for reversible solid-state transitions involving nitro torsion. Chemistry of Materials, 32(18), pp.7754-7765.
[11] Almeida e Sousa, L., Reutzel-Edens, S.M., Stephenson, G.A. and Taylor, L.S., 2015. Assessment of the amorphous “solubility” of a group of diverse drugs using new experimental and theoretical approaches. Molecular pharmaceutics, 12(2), pp.484-495.
[12] Yao, X., Henry, R.F. and Zhang, G.G., 2023. Ritonavir form III: A new polymorph after 24 years. Journal of pharmaceutical sciences, 112(1), pp.237-242.
[13] Qiu, Y., Chen, Y., Zhang, G.G., Yu, L. and Mantri, R.V. eds., 2016. Developing solid oral dosage forms: pharmaceutical theory and practice. Academic press.
[14] Wang, Y., Du, S., Wu, S., Li, L., Zhang, D., Yu, B., Zhou, L., kiflegiorgis Bekele, H. and Gong, J., 2017. Thermodynamic and molecular investigation into the solubility, stability and self-assembly of gabapentin anhydrate and hydrate. The Journal of Chemical Thermodynamics, 113, pp.132-143.
[15] Wen, H., Wang, C. and Sun, C.C., 2019. Fast determination of phase stability of hydrates using intrinsic dissolution rate measurements. Crystal Growth & Design, 19(10), pp.5471-5476.
[16] Li, Y., Chow, P.S., Tan, R.B. and Black, S.N., 2008. Effect of water activity on the transformation between hydrate and anhydrate of carbamazepine. Organic Process Research & Development, 12(2), pp.264-270.
[17] Liu, C., Dang, L., Bai, W. and Wei, H., 2013. Facile method for the prediction of anhydrate/hydrate transformation point. Industrial & Engineering Chemistry Research, 52(46), pp.16506-16512.
[18] Ticehurst, M.D., Storey, R.A. and Watt, C., 2002. Application of slurry bridging experiments at controlled water activities to predict the solid-state conversion between anhydrous and hydrated forms using theophylline as a model drug. International journal of pharmaceutics, 247(1-2), pp.1-10.
[19] Liu, C., Dang, L., Tong, Y. and Wei, H., 2013. Influence of polymorphs on the transformation water activity of theophylline. Industrial & Engineering Chemistry Research, 52(42), pp.14979-14983.
[20] Liu, C., Dang, L., Bai, W., Wang, R. and Wei, H., 2014. Solid–liquid equilibrium of theophylline in solvent mixtures. Journal of Chemical & Engineering Data, 59(2), pp.263-268.
[21] Qu, H., Louhi-Kultanen, M. and Kallas, J., 2006. Solubility and stability of anhydrate/hydrate in solvent mixtures. International journal of pharmaceutics, 321(1-2), pp.101-107.
[22] Hong, R.S., Miglani Bhardwaj, R., Henry, R., Mattei, A., Diwan, M., Thomas, A., Danzer, G.D. and Sheikh, A.Y., 2021. Distinct hybrid hydrates of paritaprevir: Combined experimental and computational assessment of their hydration–dehydration behavior and implications for regulatory controls. Crystal Growth & Design, 22(1), pp.726-737.
[23] Hong, R.S., Mattei, A., Sheikh, A.Y. and Tuckerman, M.E., 2022. A data-driven and topological mapping approach for the a priori prediction of stable molecular crystalline hydrates. Proceedings of the National Academy of Sciences, 119(43), p.e2204414119.
[24] Firaha, D., Liu, Y.M., van de Streek, J., Sasikumar, K., Dietrich, H., Helfferich, J., Aerts, L., Braun, D.E., Broo, A., DiPasquale, A.G. and Lee, A.Y., 2023. Predicting crystal form stability under real-world conditions. Nature, 623(7986), pp.324-328.
[25] Lawrence, X.Y., Carlin, A.S., Amidon, G.L. and Hussain, A.S., 2004. Feasibility studies of utilizing disk intrinsic dissolution rate to classify drugs. International journal of pharmaceutics, 270(1-2), pp.221-227.

[26] Reboul, J.P., Cristau, B., Soyfer, J.C. and Astier, J.P., 1981. 5H-Dibenz [b, f] azepinecarboxamide-5 (carbamazepine). Acta Crystallographica Section B: Structural Crystallography and Crystal Chemistry, 37(10), pp.1844-1848.
[27] Harris, R.K., Ghi, P.Y., Puschmann, H., Apperley, D.C., Griesser, U.J., Hammond, R.B., Ma, C., Roberts, K.J., Pearce, G.J., Yates, J.R. and Pickard, C.J., 2005. Structural studies of the polymorphs of carbamazepine, its dihydrate, and two solvates. Organic process research & development, 9(6), pp.902-910.
[28] Fucke, K., McIntyre, G.J., Wilkinson, C., Henry, M., Howard, J.A. and Steed, J.W., 2012. New insights into an old molecule: interaction energies of theophylline crystal forms. Crystal growth & design, 12(3), pp.1395-1401.
[29] Majodina, S., Ndima, L., Abosede, O.O., Hosten, E.C., Lorentino, C.M., Frota, H.F., Sangenito, L.S., Branquinha, M.H., Santos, A.L. and Ogunlaja, A.S., 2021. Physical stability enhancement and antimicrobial properties of a sodium ionic cocrystal with theophylline. CrystEngComm, 23(2), pp.335-352.
[30] Perdew, J. P.; Burke, K.; Ernzerhof, M. Generalized gradient approximation made simple. Phys. Rev. Lett. 1996, 77 (18), 3865−3868.
[31] Neumann, M. A.; Perrin, M.-A. Energy ranking of molecular crystals using density functional theory calculations and an empirical van der Waals correction. J. Phys. Chem. B 2005, 109 (32), 15531−15541.
[32] Kresse, G.; Furthmüller, J. Efficient iterative schemes for abinitio total-energy calculations using a plane-wave basis. Phys. Rev. B: Condens. Matter Mater. Phys. 1996, 54 (16), 11169.
[33] Kresse, G.; Hafner, J. Ab-initio molecular-dynamics for liquidmetals. Phys. Rev. B: Condens. Matter Mater. Phys. 1993, 47 (1), 558−561.
[34] Kresse, G.; Hafner, J. Ab-initio molecular-dynamics simulationof the liquid-metal amorphous-semiconductor transition in germanium. Phys. Rev. B: Condens. Matter Mater. Phys. 1994, 49 (20),14251.
[35]H.J. Zhu, Influence of water activity in organic solvent + water mixtrues on the nature of the crystallizing drug phase. 1. Theophylline
[36] F. Golles, Monatsh. Chem. 1961, 92, 981-991. Title: Examination and calculation of thermodynamic data from experimental data. I. The numerical integration of the vapor-pressure curves of the system methanol-water
[37] international crystial tables of numerical data, physics, chemistry, and technology, vol 3, p290
[38] Shefter, E. and Higuchi, T., 1963. Dissolution behavior of crystalline solvated and nonsolvated forms of some pharmaceuticals. Journal of Pharmaceutical Sciences, 52(8), pp.781-791.
[39] De Smidt, J.H., Fokkens, J.G., Grijseels, H. and Crommelin, D.J., 1986. Dissolution of theophylline monohydrate and anhydrous theophylline in buffer solutions. Journal of pharmaceutical sciences, 75(5), pp.497-501.
[40] Rodríguez-Hornedo, N., Lechuga-Ballesteros, D. and Wu, H.J., 1992. Phase transition and heterogeneous/epitaxial nucleation of hydrated and anhydrous theophylline crystals. International journal of pharmaceutics, 85(1-3), pp.149-162.
[41] Chen, S., Gao, Y., Lou, X., Henry, R.F., Stolarik, D.F., Lipert, M.P., Sheikh, A.Y. and Zhang, G.G., 2022. Overcoming Bioavailability Challenges of Dasabuvir and Enabling a Triple-Combination Direct-Acting Antiviral HCV Regimen through a Salt of Very Weak Acid for Oral Delivery. Molecular Pharmaceutics, 19(7), pp.2367-2379.
[42] Braun, D.E., Gelbrich, T., Kahlenberg, V. and Griesser, U.J., 2014. Insights into hydrate formation and stability of morphinanes from a combination of experimental and computational approaches. Molecular pharmaceutics, 11(9), pp.3145-3163.